Since January 2020 Elsevier has created a COVID-19 resource centre with free information in English and Mandarin on the novel coronavirus COVID-19. The COVID-19 resource centre is hosted on Elsevier Connect, the company's public news and information website.

Biochemical and Biophysical Research Communications 579 (2021) 69–75

Contents lists available at ScienceDirect

Biochemical and Biophysical Research Communications

journal homepage: www.elsevier.com/locate/ybbrc

SARS-CoV-2 spike protein receptor-binding domain N-glycans facilitate viral internalization in respiratory epithelial cells

Luping Zheng [a], Yingxin Ma [a], Minghai Chen [a], Guoqiang Wu [a], Chuang Yan [a], Xian-En Zhang [a, b, *]

[a] Shenzhen Institute of Synthetic Biology, Shenzhen Institutes of Advanced Technology, Chinese Academy of Sciences, Shenzhen, China
[b] National Key Laboratory of Biomacromolecules, CAS Center for Biological Macromolecules, Institute of Biophysics, Chinese Academy of Sciences, Beijing, China

ARTICLE INFO

Article history:
Received 26 August 2021
Received in revised form
19 September 2021
Accepted 22 September 2021
Available online 23 September 2021

Keywords:
SARS-CoV-2 spike RBD
N-glycosite mutation
Viral early infection
RBD neutralizing Antibody

ABSTRACT

N-glycosylation plays an important role in the pathogenesis of viral infections. However, the role of SARS-CoV-2 RBD N-glycosylation in viral entry remains elusive. In this study, we expressed and purified N331 and N343 N-glycosite mutants of SARS-CoV-2 RBD. We found that de-glycosylation at N331 and N343 drastically reduces the RBD binding to ACE2. More importantly, based on qualitative and quantitative virology research methods, we show that the mutation of RBD N-glycosites interfered with SARS-CoV-2 internalization rather than attachment potentially by decreasing RBD binding to the receptors. Also, the double N-glycosites mutant (N331 + N343) showed significantly increased sensitivity against the designated RBD neutralizing antibodies. Taken together, these results suggest that N-glycosylation of SARS-CoV-2 RBD is not only critical for viral internalization into respiratory epithelial cells but also shields the virus from neutralization. It may provide new insights into the biological process of early-stage SARS-CoV-2 infection with potential therapeutic implications.

1. Introduction

Since 2020, the coronavirus disease 2019 (COVID-19), a pandemic caused by the novel coronavirus (SARS-CoV-2), has posed an unprecedented threat to the global economy and people's lives. Huge efforts have been made to understand the mechanism of virus infection [1], develop anti-viral drugs, and vaccines based on the acquired knowledge [2–4].

N-glycosylation, the dominant post-translational modification of glycoproteins, had been related to the early infection process, especially for viral entry [5,6]. About SARS-CoV-2, a site-specific glycan analysis of the recombinant SARS-CoV-2 S revealed two N-glycosylation sites, N331 and N343, on the RBD of the S1 subunit [7]. Cryo-EM structure-based mapping suggests that these two are in the vicinity of ACE2 receptor binding sites [7]. Moreover, deletion of both N331 and N343 glycosylation drastically reduces viral infectivity, signifying the importance of N-glycosylation at these sites [8]. However, the role of S protein RBD N-glycans in the entry stage, specifically in viral attachment and internalization process, of SARS-CoV-2 infection remains undocumented. Herein, we analyze and discuss the glycopeptide pattern of the recombinant RBD of S1 protein. We examine S1 RBD N-glycosite mutants (*N-mut*) binding to recombinant ACE2 protein *in vitro*. Furthermore, pseudovirions carrying RBD N-glycosite mutant S were successfully assembled to investigate the role of RBD N-glycosylation in viral attachment and internalization in respiratory epithelial cells. Also, we examined the change in sensitivity of RBD N-glycosite mutants towards RBD neutralizing antibodies.

2. Materials and methods

2.1. Cell culture

Human HEK 293T (ATCC), human pulmonary alveolar epithelial cell (HPAEpic; ScienCell), and human nasal epithelial cell (HNEpc; PromoCell) were maintained in DMEM with 10% fetal bovine serum (FBS) at 37 °C and 5% CO_2.

* Corresponding author. Institute of Biophysics, Chinese Academy of Sciences, Beijing, 100101, China.
E-mail address: zhangxe@ibp.ac.cn (X.-E. Zhang).

https://doi.org/10.1016/j.bbrc.2021.09.053

2.2. Mutants and plasmid construction

SARS-CoV-2 S N-glycosite mutants, prepared by overlap PCR from a *SARS-CoV-2 S* containing plasmid [9], were introduced into pcDNA3.1(+) vector. The SARS-CoV-2 S1 N-glycosite mutants were cloned from SARS-CoV-2 S *N-mut* with a C-terminal octa-histidine tag. The corresponding primers for plasmid construction are listed in Table S1. HIV-1 (△env), originated from pNL4-3-KFS and pNL4-3-Luc plasmids, was used to assemble viral particles. Plasmid pcDNA3.1-VSV-G was used to encode Vesicular Stomatitis Virus (VSV) envelope G glycoprotein.

2.3. Expression and purification of SARS-CoV-2 S1

HEK 293 T cells were plated in a 15 cm dish. The cells were transfected with Lipofectamine™ 3000 and cultivated for 48 h. Then, the cells were harvested and resuspended in 2 mL non-denaturing lysis buffer on ice. The lysate was centrifuged at 13000 g for 5 min and the supernatants were mixed with Beyo-Gold™ His-tag Purification Resin. The recombinant S1 and S1 *mut* were purified using the His-tag Protein Purification Kit (Bayotime). The eluate was further purified and concentrated with a 50 kDa centrifugal filter unit (Millipore). Sample purity was also validated by SDS-PAGE.

2.4. Determination of ACE2 binding to S1

A 96 wells plate (Acro Biosystems), pre-coated with streptavidin, was normalized to RT. The wells were blocked at 37 °C for 1 h. Then, 0.1 μg biotinylated human ACE2 (Acro Biosystems) was added to each well, and the incubation was performed for 1 h at 37 °C. Next, 100 μL of 15.6–500 ng/mL recombinant S1, S1 *N-mut* and SARS-CoV-2 Spike S2 (negative control) were added to each well with incubation for 1 h at 37 °C. These were subsequently treated with SARS-CoV-2 S1 antibody (1:20000) and HRP anti-rabbit IgG at 37 °C for 1 h, respectively. Then, after incubation with tetramethylbenzidine substrate, the reaction was terminated with a stop solution. The absorbance of each well was determined at 450 nm using a microplate reader.

2.5. Pseudovirions preparation

Pseudovirions were produced by co-transfection of HEK 293T cells with pNL4-3-KFS and plasmids encoding SARS-CoV-2 S, SARS-CoV-2 S *mut,* or VSV-G. After 48 h of transfection, the filtered supernatants were incubated with 20% PEG-20000 in saline (1:1) for 16 h at 4 °C. Then, the mixture was centrifuged at 9000 rpm for 20 min, and virus pellets were resuspended in 300 μL Opti-MEM Medium (Gibco). Supernatants collected from Lipofectamine™ 3000 transfected HEK 293T culture were processed the same way as viral stock and used as mock control. To label viral membranes and lipids, the pseudovirions were stained with Vybrant DiO for 1 h at 37 °C before concentration.

2.6. Viral attachment and internalization assay

HPAEpic and HNEpc were plated on glass-bottom dishes before infection with pseudo-VSV-G or pseudo-SARS-CoV-2 S/S *N-mut* pseudovirus. For viral attachment, the cells in each group were incubated with respective pseudovirion (dose equivalent to 1 μg of p24) at 4 °C for 30 min. Then, a part of the cells was transferred to 37 °C and cultured for 1 h to initiate internalization. The residual pseudovirions on the cell surface were removed by trypsin treatment (0.01%) for 2 min at 37 °C. Fluorescence imaging and quantitative real-time PCR were used for qualitative and quantitative assessment of viral attachment and internalization.

2.7. Fluorescence imaging

Dio-labeled virions or infected cells were washed with PBS, fixed with freshly prepared 4% paraformaldehyde at RT for 15 min, and permeabilized with 0.1% Triton X-100 for 15 min (for the cells of viral internalization group only). Next, the virions or cells were incubated in 10% FBS, and then incubated with antibody against SARS-CoV-2 S1, VSV-G, followed by secondary antibodies (Alexa Fluor 555-conjugated IgG). The dual-labeled virions were considered as positive and infective pseudovirus. The sample fluorescence of virions or infected cells was monitored with an ECLIPSE Ti confocal system (Nikon, Co.) using a 60 X, 1.4 NA oil immersion objective lens. The images were analyzed with ImageJ software.

2.8. Quantitative real-time PCR (qRT-PCR)

Total RNA was extracted from purified virus or harvested cells using RNA extraction kit, respectively. Then, qRT-PCR was performed to determine viral RNA copy numbers using HiScript II U + One Step qRT-PCR Probe Kit (Vazyme) in the qTOWER^3 Real-Time PCR System (Analytik Jena). Primers and TaqMan probe targeted to the HIV-1 LTR region are shown in Table S2. Viral RNA copy numbers were calculated using a standard curve generated by serial dilutions of already quantified viral RNA PCR control of pseudo-SARS-CoV-2. The standard sample was absolutely quantified using a droplet digital PCR system (Bio-Rad) with same primers and probe mentioned above.

2.9. SARS-CoV-2 RBD neutralization assay

Recombinant SARS-CoV-2 S1 or S1 *N-mut* (0.1 μg/well) was coated on a 96-well plate. Then, serially double-fold diluted neutralizing antibody VHH72 (0.625 ng/mL-20 ng/mL, R&D SYSTEMS) [10] or AS35 (0.5 ng/mL-16 ng/mL, Acro Biosystems) [11] was added and incubated at 37 °C for 1 h, followed by addition of HRP conjugated goat anti-human IgG (Abbkine). After completion of the chromogenic reaction, sample OD450 values were recorded.

Next, HNEpc and HPAEpic (100 μL, 1×10^4 cells/well) were seeded into a white bottom 96-well micro-plate. SARS-CoV-2 S/S *N-mut* and VSV-G pseudovirions, assembled from a pNL4-3-Luc plasmid carrying the *luciferase* gene, were pre-incubated with 2.5 μg/mL S RBD neutralizing antibody for 1 h on ice. Then, the virus-antibody mixture was added to cells and incubated at 37 °C for 2 h. Viral internalization efficiency was estimated based on the luciferase activity using the Bright-Lumi™ Firefly Luciferase Assay Kit (Beyotime) at 24 hpi.

2.10. Statistical analysis

All results are expressed as means ± standard deviations. The statistical significance of differences between groups was analyzed by t-tests or one-way analysis of variance (ANOVA) using the SPSS Statistics 22 program (SPSS, Inc.).

3. Results

3.1. SARS-CoV-2 S RBD N-glycosite mutation decreased S1 binding to ACE2

We constructed S1 and S1 RBD *N-mut* to investigate the role of two N-glycosites for S1 interaction with ACE2. All the wild type (WT) and mutants were recombinantly expressed in HEK 293T cells and the His-tag protein products were purified, concentrated, and

examined by SDS-PAGE (Fig. 1A). The purified proteins were also verified by Western blotting using specific anti-SARS-CoV-2 S1 antibodies. In the mutants, de-glycosylation of the RBD N-glycosite(s) is evident by a change in protein molecular weight (Fig. 1A). Subsequently, the purified S1/S1 *N-mut* were tested for binding towards viral receptor ACE2 by a modified ELISA. We found that the binding of all constructs followed an S1 concentration-dependent pattern. Obvious differences in binding between S1/S1 *N-mut* and ACE2 were observed starting from 62.5 ng/mL of recombinant S1/S1 *N-mut* up to 500 ng/mL (Fig. 1B). Notably, the binding between WT S1 and recombinant ACE2 was highly stable; however, the double de-glycosylation (N331Q + N343Q) drastically reduced the binding(Fig. 1B and C). The respective single deletions also reduced the binding, albeit mildly, compared to the N331Q + N343Q (Fig. 1B and C).

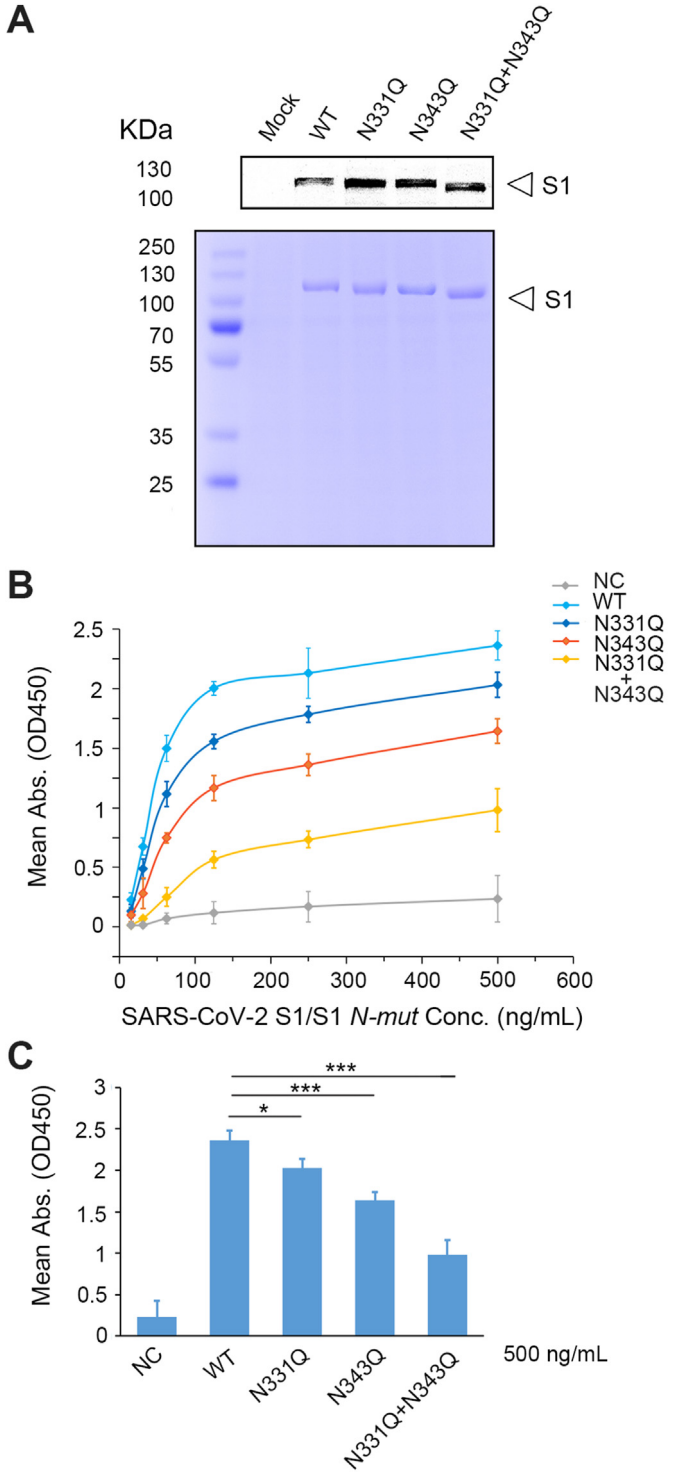

Fig. 1. The binding between recombinant SARS-CoV-2 S1/S1 *N-mut* and ACE2. (A) SDS-PAGE and Western blotting validation of SARS-CoV-2 S1/S1 *N-mut* expressed in HEK 293T cells. (B) ELISA reveals altered binding of serially diluted SARS-CoV-2 S1 *N-mut* for streptavidin coupled biotinylated ACE2 protein. (C) Absorbance for each protein at the 500-ng/mL concentration. Error bars show the standard deviations calculated from three biological repeats. WT: wild type; NC: negative control; *, $P \leq 0.05$; ***, $P \leq 0.001$.

3.2. Glycopeptide analysis of SARS-CoV-2 S RBD

The site-specific N-glycosylation profile of WT SARS-CoV-2 S1 was analyzed by liquid chromatography with tandem mass spectrometry (LC-MS/MS), and the glycan compositions were determined for 10 N-linked glycan sites, excluding 3 sites without N-glycosylation (N17, N61, and N74) (Fig. S1A). After data analysis of glycan compositions, we determined microheterogeneity at each of the 10 N-glycosites, including 2 in RBD. Firstly, we investigated the types of N-glycans. Based on branching and monosaccharide composition, the glycans were assigned into oligomannose, hybrid, and complex-type glycosylation. We found that the N-glycans at N331 and N343 were of complex-type identical to total S1. Both the RBD N-glycosites were decorated with negligible high-mannose structures (<1%). Besides, 7.1 and 9.5% of hybrid-type glycans and 10 and 0.6% of unoccupied glycans were detected at N331 and N343, respectively (Fig. S1B). We next focused on the N-glycans structures and compositions of the two RBD N-glycosites. We found that the branching from pentasaccharide core was primarily biantennary-type, approximately up to 60%, both at N331 and N343. Also, partially bisected and some triantennary-type glycans were found. Notably, relative abundance analysis revealed a high abundance of fucosylation on N331 and N343, with 92 and 99% of detected glycans bearing fucose, respectively. About 15 and 21% of the glycans at N331 and N343 contained sialic acid residue, respectively (Figs. S1C–D). The N331 and N343 N-glycans were sorted by their relative abundances and the top 10 are shown with structures in Figs. S1E–F. The identical highly abundant glycans were also found at both N331 and N343, implying a similar function of these two RBD N-glycosites. Furthermore, each of the top 10 most prevalent N-glycans carried fucosylation either on the core or branch, consistent with the high abundance of fucosylation in total N-glycans analysis. Notably, HexNAc(4)Hex(5)Fuc(1)NeuAc(1), accounting for the largest abundance at N331 and the third-highest at N343, contained terminal sialic acid for broad biological activity *in vivo* (Figs. S1E–F).

3.3. N- glycosylation of SARS-CoV-2 RBD is essential for viral internalization but not for attachment

Pseudovirions of SARS-CoV-2 were characterized by negative staining using transmission electron microscopy (TEM). The round-shaped virus particles had an average size of 100 nm (Fig. S2A). The expression of S and G proteins was confirmed by Western blotting (Figs. S2B–C). Also, to determine the effect of fluorescent labeling on viral infectivity, the pseudovirions with/without fluorescence were analyzed by luciferase assay at 24 h post infection (hpi). The results showed that DiO-labelling did not impair the virus activity (Figs. S2D and E). Pseudo-SARS-CoV-2 S/S *N-mut* and Pseudo-VSV-G were overlaid onto coverslips and stained for immunofluorescence (IF) with the anti-S (Fig. S2F; Fig. S3) or anti-VSV-G antibodies (Fig. S2G). The lipid envelope of the pseudo-virus was labeled with

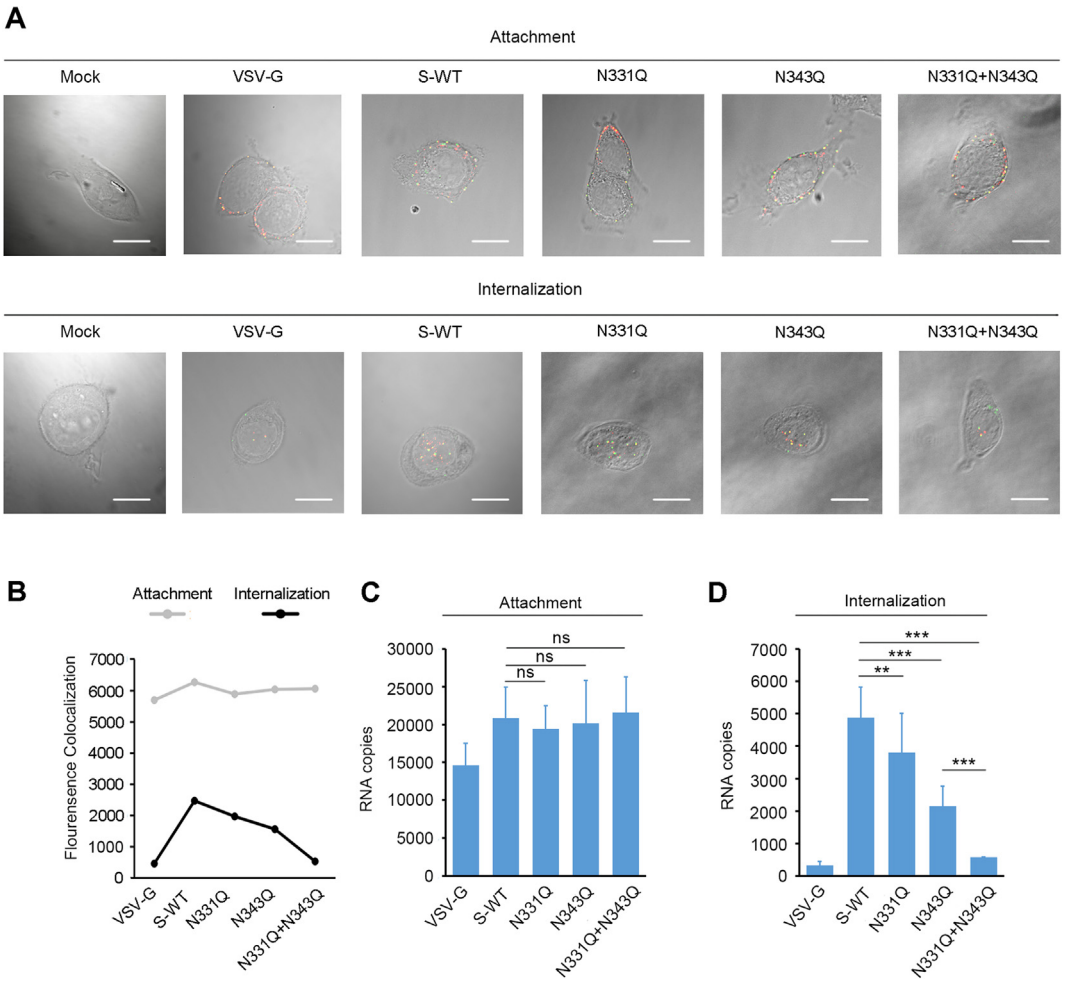

Fig. 2. The attachment and internalization of pseudo-SARS-CoV-2 in HNEpc. (A) The representative fluorescence images showing attachment and internalization of pseudo-SARS-CoV-2 S and S *N-mut*. Scale bar: 20 μm. (B) Statistical analysis of viral attachment and internalization. 300 host cells were randomly selected for statistical analysis in each group. (C and D) Quantitative analysis of viral attachment (C) and internalization (D) by qRT-PCR. Error bars show standard deviations among three biological repeats. **, $P \leq 0.01$; ***, $P \leq 0.001$.

DiO. Notably, the majority of it co-localized with the S/S *N-mut* or VSV-G. This demonstrated the successful incorporation of SARS-CoV-2 S/S *N-mut* or VSV-G proteins into the pseudovirions (Figs. S2F and G, and Fig. S3).

In HNEpc, after 30 min of co-incubation with pseudo-SARS-CoV-2 S/S *N-mut* or pseudo-VSV-G (control) at 4 °C, all the dual-labeled pseudovirions with or without mutation could attach onto the cell surface with similar efficiency (Fig. 2A, upper panel; Fig. 2B). This was also evident by the respective RNA copies in the cells (Fig. 2C). Next, viral internalization was activated by changing the temperature to 37 °C. Interestingly, the internalization efficiency of N331Q + N343Q was dramatically lower than the S-WT, similar to that of pseudo-VSV-G (control). The internalization of the single mutant N331Q or N343Q was also lower, about 23 and 56% of the S-WT, respectively (Fig. 2D). These findings are in agreement with the results of fluorescence imaging and co-location analysis (Fig. 2A, lower panel; Fig. 2B). The attachment and internalization of pseudo-SARS-CoV-2 were also tested in HPAEpic. Here too, we found similar patterns as in HNEpc (Fig. 3). The qPCR results indicated that internalization of N331Q, N343Q, and the double mutant decreased by ~37, 57, and 89%, respectively, compared with S-WT (Fig. 3D). Notably, though the viral attachment onto HNEpc and HPAEpic was of a similar level, the internalization efficiency showed a noticeable decrease in all groups in HPAEpic (Figs. 2B and 3B). The low internalization efficiency of pseudo-VSV-G compared with pseudo-SARS-CoV-2 WT suggest that the entry of the latter was indeed mediated by the S protein interaction with the receptors on these respiratory epithelial cells. Also, only the pseudovirions dual-labeled with DiO and specific antibodies were considered as positive viral particles.

To further validate these results, we examined the role of total virus surface N-glycans in viral attachment assay in respiratory epithelial cells. Pseudo-SARS-CoV-2 was treated with peptide-N-glycosidase F (PNGase F) and de-N-glycosylation was verified by PHA-L lectin blotting (Fig. S4A). When these were tested in attachment assay, only a very few de-N-glycosylated viral particles could bind to the surface of HNEpc or HPAEpic (Figs. S4B and C). Also, the viral RNA copies decreased significantly compared to the control sample (Figs. S4D and E). It suggested that the viral surface N-glycans were the predominant factor and indeed responsible for viral attachment and not the RBD N-glycans.

3.4. SARS-CoV-2 S RBD N-glycans function as "glycan shields"

Two commercially available potent SARS-CoV-2 RBD neutralizing antibodies, VHH72 (R&D) and AS35 (Acro Biosystems), were

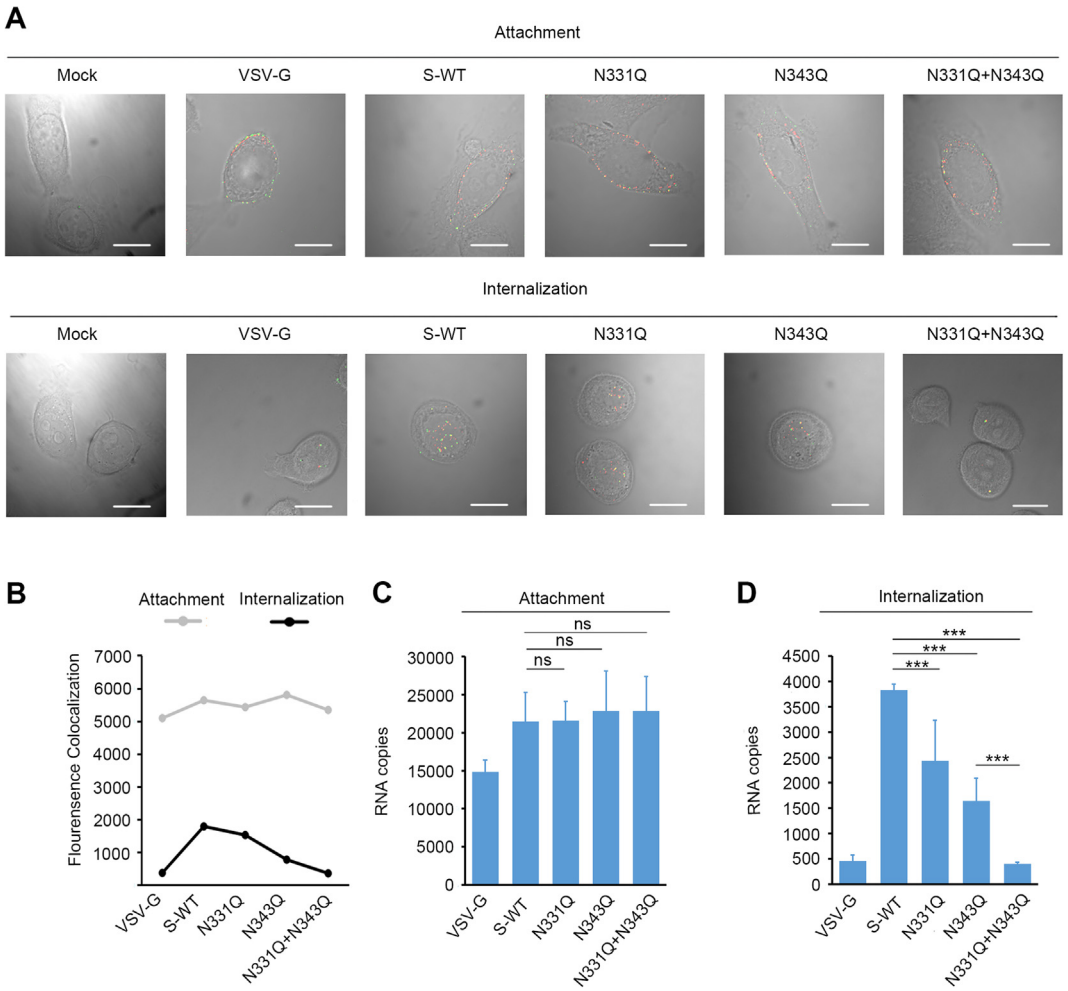

Fig. 3. The attachment and internalization of pseudo-SARS-CoV-2 in HPAEpic. (A) The representative fluorescence image showing the attachment and internalization of pseudo-SARS-CoV-2 S and S *N-mut*. Scale bar: 20 μm. (B) Statistical analysis of viral attachment and internalization. 300 host cells were randomly selected in each group. (C and D) Quantitative analysis of viral attachment (C) and internalization (D) by qRT-PCR. Error bars show standard deviations in three biological repeats. **, $P \leq 0.01$; ***, $P \leq 0.001$.

tested against recombinant S1/S1 *N-mut* by ELISA. The results indicated that compared with S-WT, the S1 binding with double mutations with RBD neutralizing antibodies was much more impacted than that of single mutant (Fig. 4A–B). Meanwhile, pseudo-SARS-CoV-2 S/S *N-mut* and pseudo-VSV-G were also tested against these two mAb to test viral infectivity by luciferase assay. VHH72 neutralized pseudo-SARS-CoV-2 S/S *N-mut* showed decreased viral infectivity in all groups in both HNEpc and HPAEpic (Fig. 4C–F). Interestingly, the decrease was most prominent, almost undetectable RLU readings, in the case of the double mutant by ~97 and 83 fold in HNEpc and HPAEpic, respectively, compared with the one without neutralization (Fig. 4F). However, the S-WT and the two single N-glycosite mutants showed only a modest reduction compared to the double mutant, by 5.1–8.0 fold in HNEpc and 5.2–7.6 fold in HPAEpic, respectively (Fig. 4C–E). AS35 neutralization showed similar effects as of VHH72, infectivity of N331Q + N343Q decreased by ~92-fold (in HNEpc) and 64-fold (in HPAEpic) compared with the one without neutralization. In the case of two single N-glycosite mutants, infectivity decreased by 3.0–5.7 fold and 2.6–4.8 fold in HNEpc and HPAEpic, respectively (Fig. 4H–K). In contrast, the control virus, pseudo-VSV-G did not show any difference in viral infectivity regardless of mAb neutralization (Fig. 4G and L).

4. Discussion

The virus surface N-glycans play a critical role in viral pathogenesis. The heavily glycosylated spike protein of SARS-CoV-2 is vital for interaction between RBD and human cell surface receptor ACE2. We demonstrated that both RBD N-glycosites were glycosylated with complex type N-glycans, lacking high mannose structures. This is consistent with Watanabe et al. and Zhao et al. which also showed that these two RBD N-glycosites were mainly modified as complex N-glycans [7,12]. It seems that under selective pressure, these complicated and variably modified glycans structures on SARS-CoV-2 RBD could have corresponding biological functions. Besides, we showed a high abundance of fucosylation and sialylation on N331 and N343, suggesting a potential role of these monosaccharides in viral ligand-receptor interaction. On the contrary, a high ratio of high-mannose type N-glycans with simpler structure and function than complex-type in the SARS-CoV-2 RBD produced in insect cells [13] explains SARS-CoV-2 preference for higher animals, such as mammals.

It was reported that deletion of both N331 and N343 glycosylation drastically reduces SARS-CoV-2 infectivity [8]. However, the fundamental mechanism remained elusive. In this study, we found that the mutation of RBD N-glycans indeed decreased the

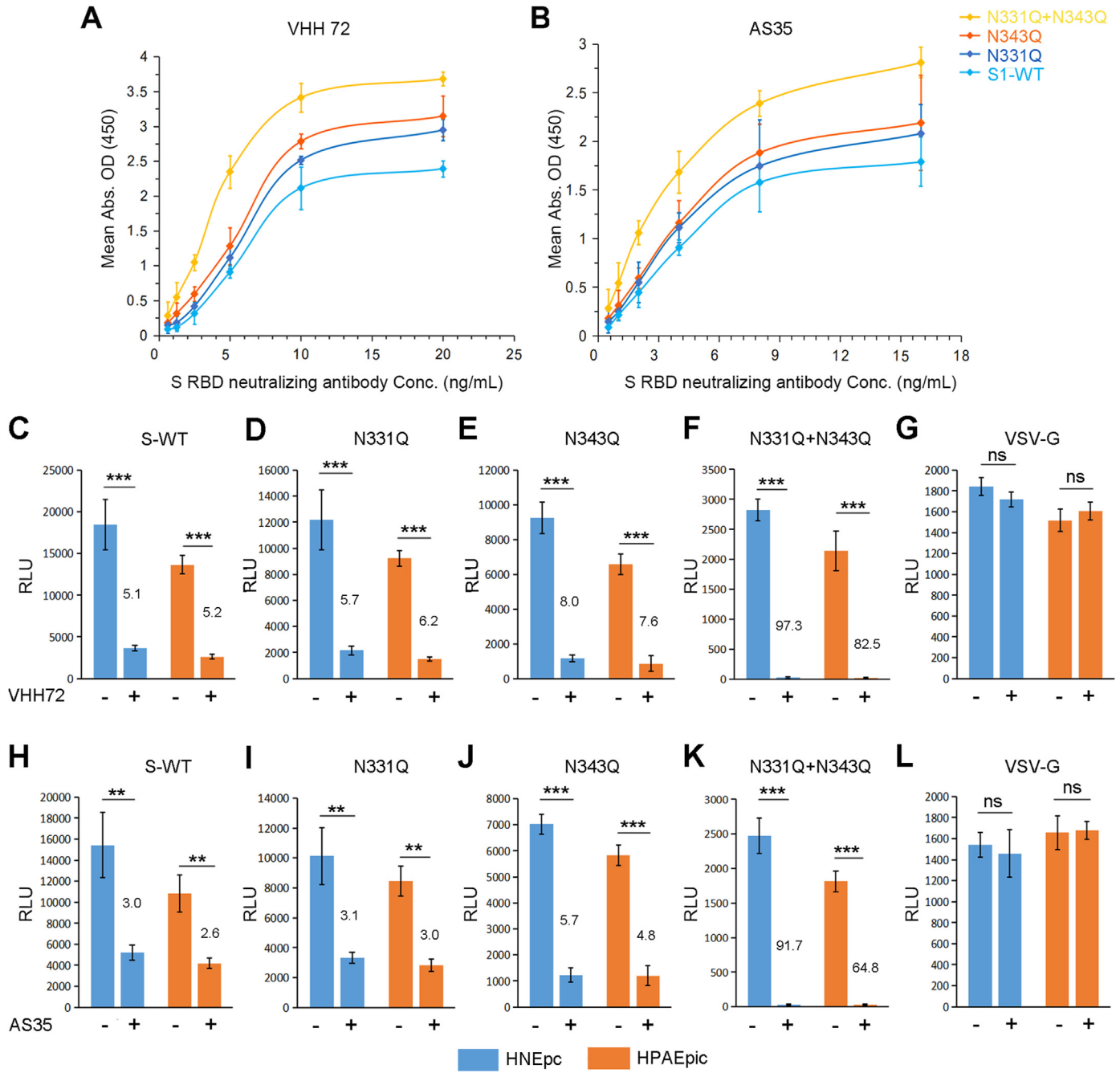

Fig. 4. SARS-CoV-2 RBD N-glycosite mutations impact binding and sensitivity towards S RBD neutralizing antibody. ELISA indicates the binding of serially diluted S RBD neutralizing antibody (A) VHH72 and (B) AS35 against pre-coated SARS-CoV-2 S/S *N-mut*. VHH72 mAb were pre-incubated with pseudo-SARS-CoV-2 S/S *N-mut* and pseudo-VSV-G (C-G) and AS35 mAb were pre-incubated with pseudo-SARS-CoV-2 S/S *N-mut* and pseudo-VSV-G (H-L) before infecting HNEpc and HPAEpic. Viral infectivity and internalization efficiency were measured by Luciferase assay after 24 h. The values above the bars denote fold changes in RLU between the groups with or without neutralization. The data (mean ± SD) are from three replicates. **, $P \leq 0.01$; ***, $P \leq 0.001$.

interaction between S1 and ACE2 showing their importance in viral entry. Moreover, we show that the reduction in infectivity mainly affected the viral internalization process rather than attachment to respiratory epithelial cells. Though virus surface N-glycans are critical for attachment [14] and our result also indicated significantly decreased attachment of de-N-glycosylated pseudo-SARS-CoV-2, the mutation of N331 and N343 did not impact the viral attachment. It seems that the remaining S protein N-glycosites or other glycoproteins on the viral membrane are enough for attachment. Also, heparan sulfate, distributed on the surface of virtually all mammalian cells, is considered an important attachment factor for SARS-CoV-2 infection [15]. The decreased viral internalization of de-N-glycosylated N331 + N343 can be for two potential reasons. Firstly, the specific monosaccharides at N331 and N343 could be involved in receptor interaction. The N331 and N343 N-glycosites shared similar glycan composition and relative abundance. The 10 most abundant glycans on these two N-glycosites were modified by core or branched-fucosylation. Also, HexNAc(4)Hex(5)Fuc(1)NeuAc(1), the dominant N-glycan at both N331 and N343 was modified with terminal sialic acid. Notably, sialylated and

fucosylated glycans are often used by various microorganisms to recognize and bind to host receptors. Viral receptor recognition and binding are the key events of early infection, especially in the viral internalization process. HIV-1 gp120 mediates infection by binding to HIV receptors. The fucosylated glycans on gp120, which recognize and bind to DC-SIGN, play a critical role in dendritic cells infection during HIV transmission [16]. NMHC-IIA is a contributing factor in viral infections. Liu et al. showed that VSV recognizes NMHC-IIA by surface sialic acids and initiates infection [17]. Shajahan et al. revealed that the RBD adjacent highly sialylated glycans at N234 and N282 determine SARS-CoV-2 binding with ACE2 receptors [18]. Very recently, Wang et al. reported that RBDs containing homogeneous N-glycans at N331 and N343 without core fucose and sialic acids did not influence their binding to ACE2 [19]. Thus, the high abundance of fucosylated and sialylated glycans on N-glycosites of SARS-CoV-2 RBD could not be neglected for their role in interaction with host receptors. Given their involvement in protein folding, glycosylation significantly affects the glycoprotein conformation. We speculate that the second reason for impacted viral internalization could be altered SARS-CoV-2 RBD conformation. It seems that the two N-glycosites are critical for suitable binding conformation of the RBD region. Of note, the differential internalization efficiency of pseudo-SARS-CoV-2 in the upper and lower respiratory tract epithelial cells suggests viral tropism towards diverse cells, which may be influenced by the cell surface amount of ACE2. It is reasonable to speculate that SARS-CoV-2 infects nasal epithelial cells much easier than alveolar epithelial cells because of its aerosol or droplet transmission mode. In addition, we previously showed that the ACE2 expression of HNEpc was indeed higher than that of HPAEpic both at transcription and translation levels [9].

Though SARS-CoV-2 S glycan shields the immune response [7,20], the sensitivity of RBD N-glycans against RBD neutralizing antibodies remains ambiguous. Here, we found that the recombinant S1 *N-mut* exhibited increased binding with the two neutralizing antibodies targeting RBD epitopes, while the pseudo-SARS-CoV-2 S *N-mut* showed a lower internalization rate when was blocked with the antibodies. A similar N-glycosite mutation-induced increased antibody neutralization was also reported for HIV-1 gp120 and Nipah virus attachment glycoprotein [21,22]. The mutants N331 and N343, located in the RBD region, may affect epitope targeting by neutralizing antibodies. The RBD N-glycans likely mask the epitope targeted by the antibody, which is probably an evolutionary mechanism to protect from neutralization and maintain a high affinity for the receptors. Notably, with similar glycan compositions, the binding to the receptors or RBD neutralizing antibodies was different among N331Q, N343Q, and N331Q + N343Q. We speculate that it could be due to the varied spatial location of these two N-glycosites in RBD tertiary structure which influences protein conformation and affinity. Nevertheless, one cannot exclude the possibility that the glycans themselves can be the targets of RBD antibodies. Therefore, the N-glycosites located on the RBD epitope should be considered in the design and optimization of COVID-19 vaccines and neutralizing antibodies. A mixture of neutralizing antibodies originating from different epitopes may even be more effective.

Declaration of competing interest

The authors declare that they have no known competing financial interests or personal relationships that could have appeared to influence the work reported in this paper.

Acknowledgement

This work was supported by the Strategic Priority Research Program of the Chinese Academy of Sciences (XDB29050100), National Key Research and Development Program of China (2017YFA0205503), China Postdoctoral Science Foundation (2020M682972).

Appendix A. Supplementary data

Supplementary data to this article can be found online at https://doi.org/10.1016/j.bbrc.2021.09.053.

References

[1] M. Hoffmann, H. Kleine-Weber, S. Schroeder, et al., SARS-CoV-2 cell entry depends on ACE2 and TMPRSS2 and is blocked by a clinically proven protease inhibitor, Cell 181 (2020) 271–280.e8.
[2] J.M. Sanders, M.L. Monogue, T.Z. Jodlowski, J.B. Cutrell, Pharmacologic treatments for coronavirus disease 2019 (COVID-19): a review, J. Am. Med. Assoc. 323 (2020) 1824–1836.
[3] M. Jeyanathan, S. Afkhami, F. Smaill, et al., Immunological considerations for COVID-19 vaccine strategies, Nat. Rev. Immunol. 20 (2020) 615–632.
[4] B.F. Haynes, A new vaccine to battle Covid-19, N. Engl. J. Med. 384 (2021) 470–471.
[5] A. Beyene, A. Basu, K. Meyer, R. Ray, Influence of N-linked glycans on intracellular transport of hepatitis C virus E1 chimeric glycoprotein and its role in pseudotype virus infectivity, Virology 324 (2004) 273–285.
[6] F.L. Chu, H.L. Wen, G.H. Hou, et al., Role of N-linked glycosylation of the human parainfluenza virus type 3 hemagglutinin-neuraminidase protein, Virus Res. 174 (2013) 137–147.
[7] Y. Watanabe, J.D. Allen, D. Wrapp, et al., Site-specific glycan analysis of the SARS-CoV-2 spike, Science 369 (2020) 330–333.
[8] Q. Li, J. Wu, J. Nie, et al., The impact of mutations in SARS-CoV-2 spike on viral infectivity and antigenicity, Cell 182 (2020) 1284–1294.
[9] Y. Ma, G. Mao, G. Wu, et al., A Dual-fluorescence labeling pseudovirus for real-time imaging of single SARS-CoV-2 entry in respiratory epithelial cells, ACS Appl. Mater. Interfaces 2 (2020) 24477–24486.
[10] D. Wrapp, D. De Vlieger, K.S. Corbett, et al., Structural basis for potent neutralization of betacoronaviruses by single-domain camelid antibodies, Cell 181 (2020) 1004–1015.e15.
[11] K.S. Park, J.D. Bazzill, S. Son, et al., Lipid-based vaccine nanoparticles for induction of humoral immune responses against HIV-1 and SARS-CoV-2, J. Contr. Release 330 (2021) 529–539.
[12] P. Zhao, J.L. Praissman, O.C. Grant, et al., Virus-receptor interactions of glycosylated SARS-CoV-2 spike and human ACE2 receptor, Cell Host Microbe 28 (2020) 586–601.e6.
[13] Y. Zhang, W. Zhao, Y. Mao, et al., Site-specific N-glycosylation characterization of recombinant SARS-CoV-2 spike proteins, Mol. Cell. Proteomics 20 (2021), 100058.
[14] Y. Watanabe, T.A. Bowden, I.A. Wilson, M. Crispin, Exploitation of glycosylation in enveloped virus pathobiology, Biochim. Biophys. Acta Gen. Subj. 1863 (2019) 1480–1497.
[15] H. Chu, B. Hu, X. Huang, et al., Host and viral determinants for efficient SARS-CoV-2 infection of the human lung, Nat. Commun. 12 (2021) 134.
[16] B. Monzavi-Karbassi, P. Luo, G. Cunto-Amesty, et al., Fucosylated lactosamines participate in adhesion of HIV-1 envelope glycoprotein to dendritic cells, Arch. Virol. 149 (2004) 75–91.
[17] Y. Liu, R. Li, X.X. Chen, et al., Nonmuscle myosin heavy chain IIA recognizes sialic acids on sialylated RNA viruses to suppress proinflammatory responses via the DAP12-Syk pathway, mBio 10 (2019) e00574–19.
[18] A. Shajahan, N.T. Supekar, A.S. Gleinich, P. Azadi, Deducing the N- and O-glycosylation profile of the spike protein of novel coronavirus SARS-CoV-2, Glycobiology 30 (2020) 981–988.
[19] P. Wang, F. Ye, J. Zhao, et al., Synthetic homogeneous glycoforms of the SARS-CoV-2 spike receptor-binding domain reveals different binding profiles of monoclonal antibodies, Angew Chem. Int. Ed. Engl. 60 (2021) 12904–12910.
[20] O.C. Grant, D. Montgomery, K. Ito, R.J. Woods, Analysis of the SARS-CoV-2 spike protein glycan shield reveals implications for immune recognition, Sci. Rep. 10 (2020) 14991.
[21] S.B. Biering, A. Huang, A.T. Vu, et al., N-Glycans on the Nipah virus attachment glycoprotein modulate fusion and viral entry as they protect against antibody neutralization, J. Virol. 86 (2012), 11991–2002.
[22] W. Wang, J. Nie, C. Prochnow, et al., A systematic study of the N-glycosylation sites of HIV-1 envelope protein on infectivity and antibody-mediated neutralization, Retrovirology 10 (2013) 14.